

# Damage modelling of a TRIP steel for integrated simulation from deep drawing to crash

Dr. Dong-Zhi Sun<sup>\*</sup>, Dr. Florence Andrieux<sup>\*</sup>, Dr. Markus Feucht<sup>\*\*</sup>

<sup>\*</sup>Fraunhofer Institute for Mechanics of Materials  
Woehlerstrasse 11, 79108 Freiburg, Germany,

<sup>\*\*</sup>Daimler AG, W059 / HPC X271, 71059 Sindelfingen, Germany

## Abstract:

The local mechanical properties e.g. flow stress and fracture strain in an automotive component manufactured by deep drawing are inhomogeneous due to different local deformation degrees which affect the component behaviour under crash loading. A reasonable approach for modelling the damage behaviour of a component produced by deep drawing is a coupling between forming simulation and crash simulation. The open questions are which material model (kinematic or isotropic hardening) and which damage model should be used for an integrated simulation. Since the loading type is mainly biaxial at deep drawing and uniaxial under crash, it should be investigated how the damage development is influenced by deformation history including change of stress state. In this work the influence of triaxiality and pre-deformation on damage behaviour of a TRIP steel was characterized with different specimen tests e.g. under shear, uniaxial and biaxial tension and a damage model taking into account shear fracture and dimple rupture was developed. This damage model can also describe the influence of pre-deformation. Validation tests on an automobile component under a loading close to reality were performed and simulated with pre-strains and pre-damage mapped from a forming model to the crash model.

## Keywords:

Damage modelling, TRIP steel, material characterization, shear test, process chain, pre-deformation, loading history, component test

## 1 Introduction

In the trend of lightweight construction more and more high strength steels come to application in automotive structural components. Since the ductility of high strength steels is relatively low, damage behaviour of these materials has to be modelled in vehicle crash simulations to achieve a reliable crashworthiness prediction. The local mechanical properties e.g. flow stress and fracture strain in an automotive component manufactured by deep drawing are inhomogeneous due to different local deformation degrees which affect the component behaviour under crash loading considerably. A reasonable approach for modelling the damage behaviour of a component produced by deep drawing is a coupling between forming simulation and crash simulation [1, 2]. However, many questions are still open for this approach, e.g. how the damage behaviour is influenced by change of loading conditions from forming to crash and which material model (kinematic or isotropic hardening) and which damage model should be used for an integrated simulation.

In this work the influence of pre-strain and pre-damage caused by deep drawing on the crash behaviour of an automobile component from a TRIP steel was investigated. To study the dependence of damage on loading history, metal sheets were at first loaded under biaxial tension to different loading levels, then small tension and shear specimens were cut from the deformed sheets and loaded to final rupture. In this way the influences of loading history and triaxiality on damage behaviour were quantified. A general material model which describes kinematic hardening, anisotropy and damage was developed and implemented for forming and crash simulations. To validate the damage model component tests under bending with superimposed tension were performed and simulated. The distributions of pre-strain, pre-damage and thickness from the forming simulation were mapped onto the crash model. The results demonstrate the importance of the coupling between deep-drawing simulation and crash simulation.

## 2 Characterization of material behaviour

A steel sheet of TRIP700 with thickness of 1.8 mm was characterized with experiments on different specimens. An automobile component manufactured by deep drawing from this material was characterized with sub-sized tension specimens cut from different positions to quantify the influence of forming processes on local properties.

### 2.1 Influence of triaxiality on damage behaviour

To vary stress triaxiality shear tests, smooth and notched tension tests and biaxial tension tests were performed under static loading. Figure 1 shows the different specimens after test. Three shear specimen types (Arcan, Iosipescu and shear-tension) were compared. The stress triaxiality in the shear-tension specimens mainly depends on the angle  $\theta$  between the line connecting both notch tips and the load line [3]. The loading in the specimen with the two notch tips at the loading line ( $\theta=0^\circ$ ) is closest to pure shear. By increasing the angle  $\theta$  from  $0^\circ$  to  $90^\circ$  the loading type can be varied from pure shear to tension. Three different forms of shear specimens ( $\theta=0^\circ$ ,  $30^\circ$  and  $45^\circ$ ) were used in this investigation. The triaxiality in the specimens with an angle of  $30^\circ$  and  $45^\circ$  is similar for this material. Additionally, smooth and notched flat tension specimens with notch radii of 1 mm and 4 mm were tested. For biaxial tension Marciniak tests were performed at IBF of RWTH Aachen. A homogeneous biaxial stress state in the bottom of each specimen was found by evaluating measured local strains and the triaxiality calculated with FE simulations. Figure 1 also shows the fracture strains under different loading characterised by triaxiality. The triaxiality is defined as the ratio of the mean stress  $\sigma_m$  to the von Mises effective stress  $\sigma_e$ . The values of triaxiality for shear, uniaxial tension and biaxial tension are zero, one third and two thirds, respectively. Since local strains and triaxiality are not homogeneous in the specimens due to stress gradients or localization of deformation, FE simulations were performed to determine the fracture strains and triaxiality. The evolutions of the plastic strain and triaxiality are evaluated from the first damaged elements and are shown in Figure 1 (vertical lines) for different specimens. The values presented by triangle symbols in Figure 1 were determined by fitting the calculated load vs. displacement curve to the measured displacement at rupture. Triaxiality changes with increasing loading especially for shear-tension specimens. These results shown in Figure 1 give evidence that for this material fracture strain under shear is lower than that under uniaxial tension.

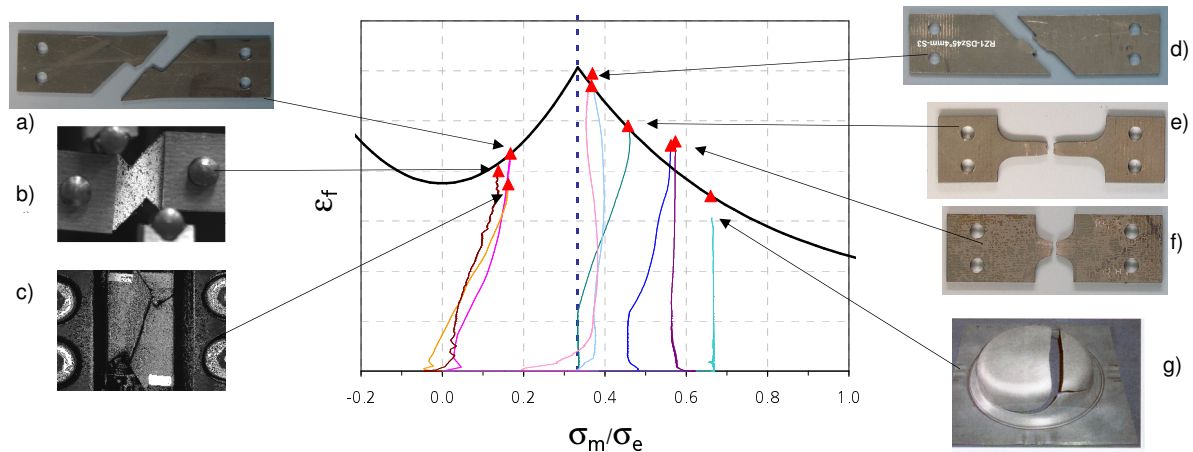


Figure 1: Fracture strain  $\epsilon_f$  as function of stress triaxiality  $\sigma_m/\sigma_e$  and loading history for different tests a) shear tension  $\theta=0^\circ$ , b) losipescu shear, c) Arcan shear, d) shear tension  $\theta=45^\circ$ , e) smooth tension, f) notched tension  $r=4$  mm, g) Marciniak biaxial tension

## 2.2 Influence of predeformation on damage behaviour

To investigate the influence of predeformation and change of triaxiality during loading on damage development sheets of TRIP700 were at first loaded under biaxial tension by means of Marciniak tests to different strain levels and then tension and shear specimens were cut from the bottom of the Marciniak specimens and loaded to rupture. Figure 2 shows a Marciniak specimen loaded to 50% of fracture strain under biaxial loading. Figure 3 compares the technical stress vs. strain curves from the original sheet and from specimens with different pre-strains under biaxial loading. The pre-deformation leads to a pronounced increase in the flow stress and a decrease in fracture strain.

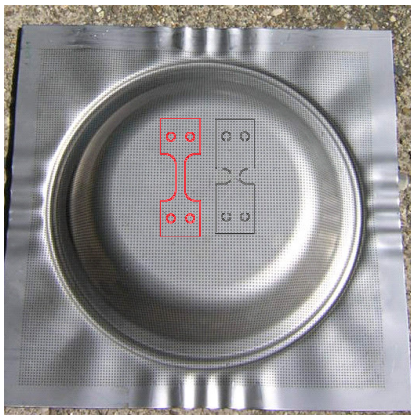


Figure 2: Smooth and notched tension specimens cut from a Marciniak specimen deformed to 50% of fracture strain

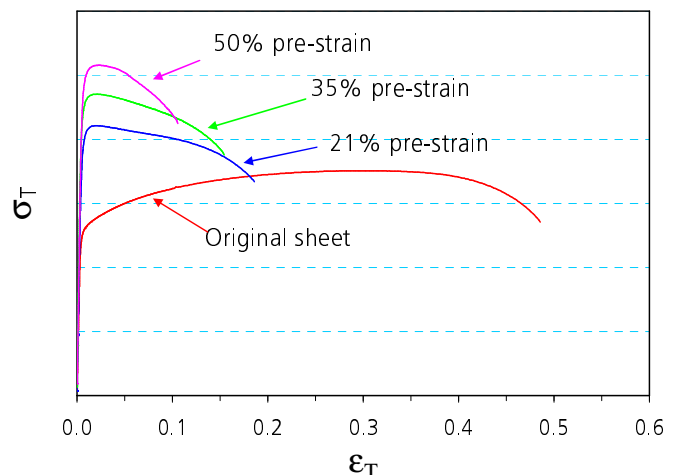


Figure 3: Measured technical stress vs. strain curves of tension specimens with and without predeformation

To identify the influence of the forming process on local properties in a real component sub-sized tension and shear specimens were cut from different positions in an automobile component of TRIP700. Figure 4 shows one position (side wall of the component) for specimen extraction. The technical stress vs. strain curves for different positions in the deep-drawn component are compared with the curves of specimens from the original sheet in three orientations in Figure 5. The distribution of pre-strains in the component is not homogeneous and therefore the flow stress and fracture strain vary in a large range. The original sheet of the TRIP700 steel shows only a very small dependence of the flow behaviour on specimen orientation.

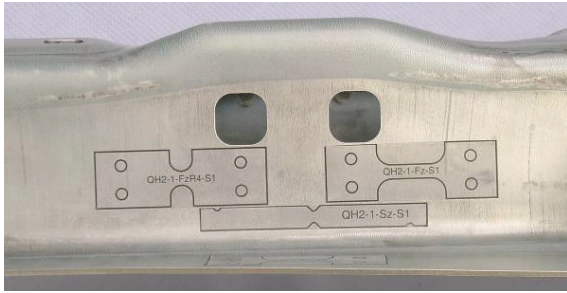


Figure 4: Extraction of sub-sized tension and shear specimens from a component after deep drawing

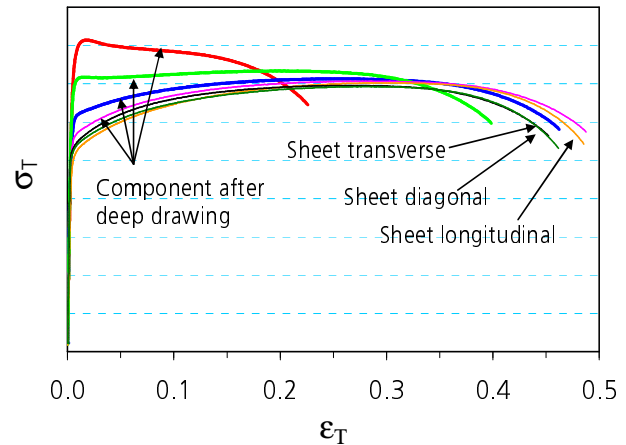


Figure 5: Measured technical stress vs. strain curves for tension specimens cut from different positions of a component compared to sheet data

### 3 Investigation of kinematic hardening

#### 3.1 Tension-compression tests

In the deep drawing process the sheet metal can be subjected to changes in the loading path e.g. locally from tension to compression then to tension. Moreover, the change from deep drawing (mainly equibiaxial) to crash (mainly uniaxial) involves change of loading path as well. For these reasons it is important to characterize the kinematic hardening. Cyclic tension-compression tests with increasing strain levels were performed. Both symmetric and asymmetric strain amplitudes were used. Additionally, to investigate the anisotropy effect of the material, specimens were cut in three directions from the sheet, namely the rolling, transverse and diagonal directions. To avoid instability of the flat specimens during compression a special specimen form and a special clamping method were used. Figure 6 shows cyclic tension-compression stress vs. strain curves for two loading cases. Based on these curves the hardening type was investigated. These curves also make clear that for this material the orientation dependency is negligible.

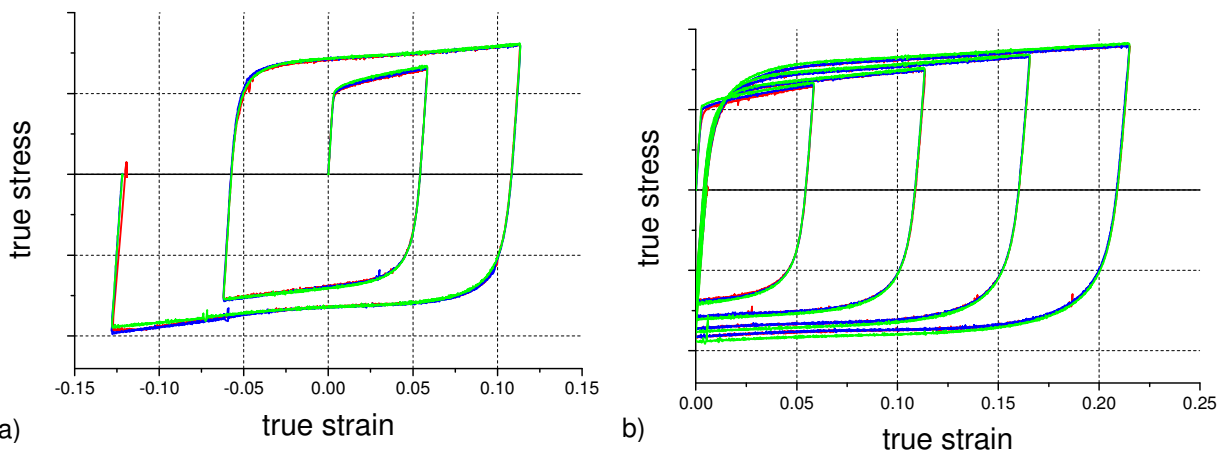


Figure 6: Stress vs. strain curves under cyclic tension-compression loadings for 3 material directions (rolling ---, transverse --- and diagonal ---) a) symmetric strain amplitude b) asymmetric strain amplitude

#### 3.2 Material model for kinematic hardening

For an integrated simulation of deep drawing and crash an elasto-plastic constitutive model was developed by using the yield function proposed by Barlat [4] for orthotropic sheet metals exhibiting

planar anisotropy with a combined isotropic-kinematic hardening model of Chaboche-type [5]. The yield function  $\phi$  is written as:

$$\phi = \sqrt[m]{\frac{1}{2} \left( a |K_1 + K_2|^m + a |K_1 - K_2|^m + (2-a) |2K_2|^m \right)} - k - R = 0 \quad (1)$$

with

$$K_1 = \frac{\tau_{xx} + h\tau_{yy}}{2}, \quad K_2 = \sqrt{\left( \frac{\tau_{xx} - h\tau_{yy}}{2} \right)^2 + \rho^2 \tau_{xy}^2} \quad (2)$$

In (1) and (2)  $\tau = \sigma - \mathbf{X}$  denotes the effective stress,  $\mathbf{X} = \mathbf{X}_1 + \mathbf{X}_2$  the total back stress,  $R = R_1 + R_2$  the total isotropic hardening and  $k$  the initial yield stress in the rolling direction.  $R_1$  and  $R_2$  are two isotropic hardening variables and  $\mathbf{X}_1$  and  $\mathbf{X}_2$  are two back stresses. The parameters  $m$ ,  $a$ ,  $h$  and  $\rho$  describe the plastic anisotropy,  $a$ ,  $h$  and  $\rho$  are obtained through the Lankford parameters  $r_0$ ,  $r_{90}$  and  $r_{45}$ . The isotropic and kinematic hardening rules are chosen according to Berstad et al. [6]. The isotropic parts of the hardening have the following evolution equations:

$$\dot{R}_k = C_{Rk} (Q_{Rk} - R_k) \dot{p} \quad k = 1, 2 \quad (3)$$

The kinematic parts of the hardening have the following evolution equations:

$$\dot{X}_{kij} = C_{Xk} \left( Q_{Xk} \frac{\tau_{ij}}{\tau_{eq}} - X_{kij} \right) \dot{p} \quad k = 1, 2 \quad (4)$$

$(C_{Rk}, Q_{Rk}, C_{Xk}, Q_{Xk})_{k=1,2}$  are eight parameters describing the hardening.  $\dot{p}$  is the plastic multiplier determined using the consistency condition.

The cyclic tests were simulated using both an isotropic and a combined isotrop-kinematic hardening law. Figure 7 makes clear that a kinematic hardening has to be taken into account to well predict the cyclic loading tests. In Figure 7 only one representative experiment has been plotted. It should also be mentioned that both models with isotropic and combined hardening cannot capture the early reyielding and the smooth curvature after the load reversal. For a better description of the experimental curve, especially after the reversal more back stress components have to be defined as explained by Lemaitre and Chaboche [5]. Figure 8 compares the yield surfaces predicted by the material models for isotropic and isotrop-kinematic hardening after a biaxial loading. The load level shown in Figure 8 corresponds to the deformation in a Marciniak specimen loaded to 50% of fracture strain (see Figure 2).

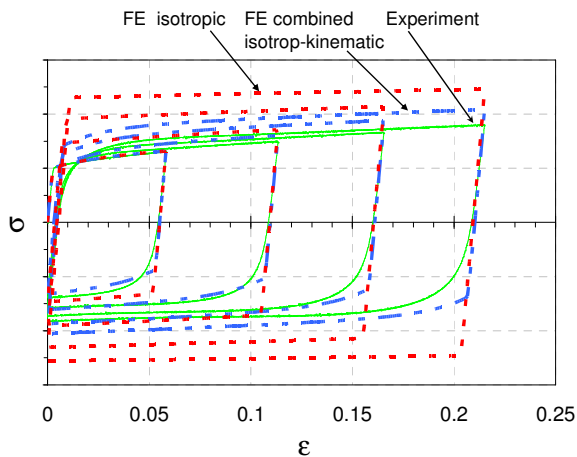


Figure 7: Cyclic tests and simulation with and without kinematic hardening.

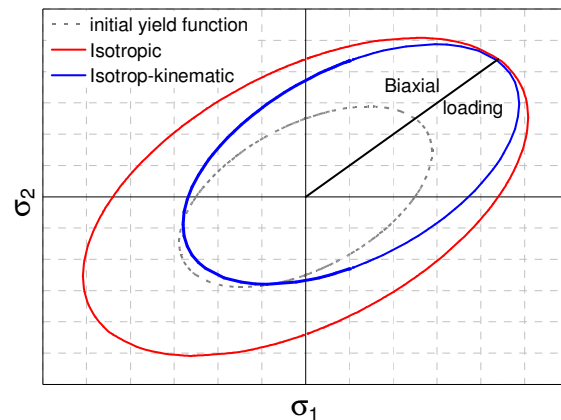


Figure 8: Yield surfaces for isotropic and isotrop-kinematic hardening after a biaxial loading

## 4 Damage modelling

Many experiments [7, 8] give evidence that both types of ductile fracture i.e. shear failure and dimple rupture can occur in a metallic component under complex loading. An important finding is that the fracture strain in shear can be well below fracture strains under significantly higher triaxialities, which is contrary to the assumption of conventional damage models like Gurson and Johnson-Cook. The curve of fracture strain vs. triaxiality shown in Figure 1 is divided into two areas for shear failure and dimple rupture and a minimum of the fracture strain lies in pure shear (zero triaxiality). The problem of the conventional damage models is that they take into account only the micro-mechanisms of void growth which is controlled by hydrostatic stress. The micro-mechanisms of shear failure are the initiation of micro-cracks at grain boundaries by shear stress through slipping between neighboring grains and subsequent extension or connection through intergranular boundaries or through transgranular slip bands [3]. Therefore, the damage development under shear is no longer tied to hydrostatic stress and should be described with deviatoric stresses [8]. Based on experimental observations and theoretical analyses in the literature, a damage concept for shear failure and dimple fracture was used in a previous work [9] and extended in this work using a general model.

### 4.1 Damage model for two failure mechanisms

The damage model proposed in this work is based on a fracture strain criterion. The fracture strain  $\varepsilon_f$  is defined as a function of the stress triaxiality  $T = \sigma_m / \sigma_e$ . The difference to the Johnson-Cook type fracture criterion [10] is that the fracture strain does not decrease monotonically with increasing triaxiality. The domain is divided into two regions for dimple rupture at high triaxialities and shear failure at low triaxialities (Figure 9). Above a triaxiality  $T_{trans}$  (which is a material parameter and is expected to be about 0.3) the failure curve proposed by Johnson-Cook (5) is used which involves three material parameters  $d_1$ ,  $d_2$  and  $d_3$ . Below  $T_{trans}$  an empirical polynomial curve (6) is proposed with a minimum at  $T=0$ .

$$T > T_{trans} \quad \varepsilon_f = (d_1 + d_2 \exp(-d_3 T)) \quad (5)$$

$$T < T_{trans} \quad \varepsilon_f = d_{shear1} + d_{shear2} |T|^{m_2} + d_{shear3} \langle -T \rangle^{m_3} \quad (6)$$

The third term in (6) is introduced to define an asymmetry in the failure strain with respect to the triaxiality, especially to account for different failure strains in tension and in compression, eventually no failure in compression at all. In equation (6)  $\langle \cdot \rangle$  denote the Macauley brackets which return the argument when positive and zero otherwise. Only the parameters  $d_{shear1}$ ,  $m_2$  and  $m_3$  have to be defined by the user for the shear region ( $T < T_{trans}$ ). The parameter  $d_{shear2}$  is calculated in the routine to ensure the continuity of the failure strain function at  $T_{trans}$ . In the model the failure strain in compression  $E_{comp}$  is a material parameter to be given by the user. The parameter  $d_{shear3}$  is calculated in the model by using the fracture strain  $E_{com}$  under uniaxial compression ( $T = -1/3$ ).

Fracture occurs when the cumulative damage parameter  $D$  defined by (7) reaches the critical value of 1. Johnson-Cook [10] proposed a linear damage accumulation. A more general non-linear damage accumulation is used here:

$$\dot{D} = \frac{n}{\varepsilon_f^n} \varepsilon_p^{n-1} \dot{\varepsilon}_p \quad (7)$$

In (7)  $\varepsilon_p$  denotes the equivalent plastic strain and the exponent  $n$  is a parameter controlling damage evolution. For constant  $\varepsilon_f$  the integration of (7) leads to  $D = (\varepsilon_p / \varepsilon_f)^n$ .

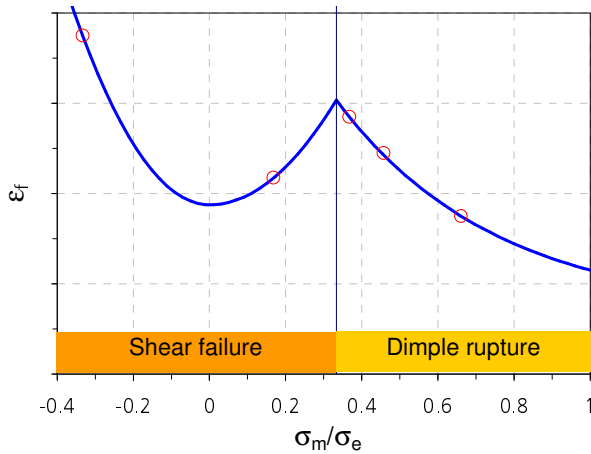


Figure 9: Fracture strain as function of triaxiality for a TRIP700 steel

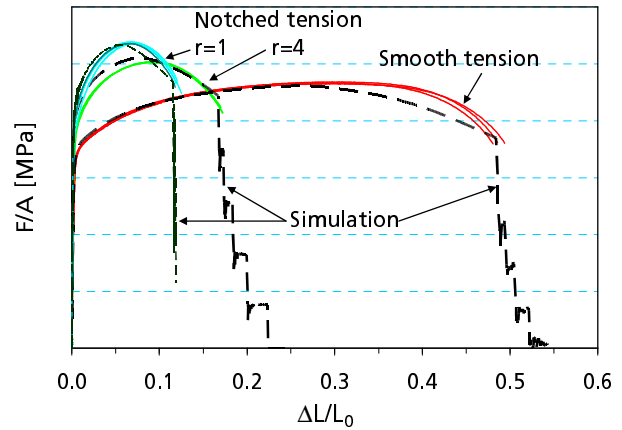


Figure 10: Measured and simulated nominal stress vs. nominal strain curves for smooth and notched tension specimens

#### 4.2 Simulation of specimen tests

The damage model described above was used to simulate all specimen tests performed in this work. The damage parameters  $d_1$ ,  $d_2$  and  $d_3$  for the region  $T > 1/3$  were determined by fitting the fracture strains of smooth and notched tension and Marciniak specimens. The damage parameters for the range  $T < 1/3$  were obtained by fitting the fracture strains of different shear tests. The sheets of the investigated TRIP700 steel do not show failure under compression. To complete the damage curve for the whole range of triaxiality relevant for crash simulation, a very high value of fracture strain was defined for uniaxial compression. The damage curve used in this work is given in Figure 1 and Figure 9.

The von Mises flow function for isotropic hardening was used for most simulations. Additionally, some experiments were simulated with the material model for isotrop-kinematic hardening described in section 3 and the results are shown in section 4.3. The measured and calculated nominal stress vs. strain curves of smooth and notched tension specimens with notch radii of 1 and 4 mm are compared in Figure 10. Figure 11 shows the measured and calculated load vs. displacement curves of shear tension tests with three specimen geometries ( $\theta = 0^\circ$ ,  $30^\circ$  and  $45^\circ$ ). In all cases the calculated displacements at fracture agree well with experimental results. Figure 12 shows the deformed meshes at beginning of rupture for two shear tension specimens ( $\theta = 0^\circ$  and  $45^\circ$ ). Due to different fractions of shear stresses the damage initiates in the centre of the specimen with  $\theta = 0^\circ$  and at the notch root of the specimen with  $\theta = 45^\circ$ .

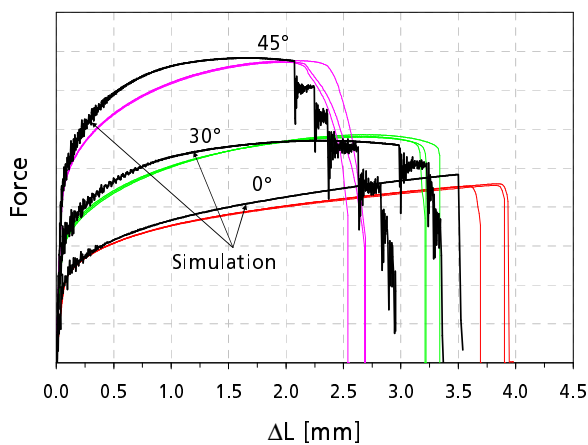


Figure 11: Measured and simulated force vs. displacement curves for three shear-tension tests ( $\theta = 0^\circ$ ,  $30^\circ$  and  $45^\circ$ )

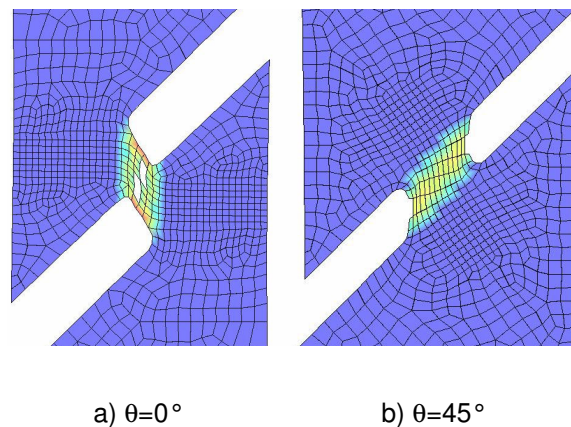


Figure 12: Distributions of effective plastic strain and damage initiation in two different shear tension specimens

Figure 13 compares the measured and calculated load vs. stamp displacement curves of Marciniak tests. To reduce friction between stamp and metal sheet many efforts have been made at the IBF of RWTH Aachen e.g. application of film, oil and fat on the specimen surfaces. The simulations show that the friction coefficient  $\mu$  has a large influence on the load, distribution of strains and damage pattern. The application of a small friction coefficient results in a good agreement between experiment and simulation. The damage pattern calculated with  $\mu=0.03$  agrees with the experimental observation (Figure 14).

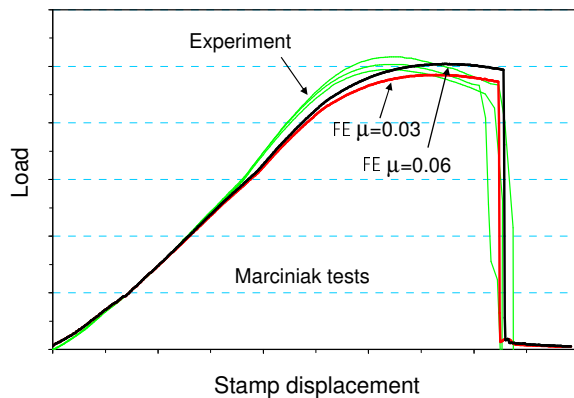


Figure 13: Measured and simulated force vs. stamp displacement curves of Marciniak tests

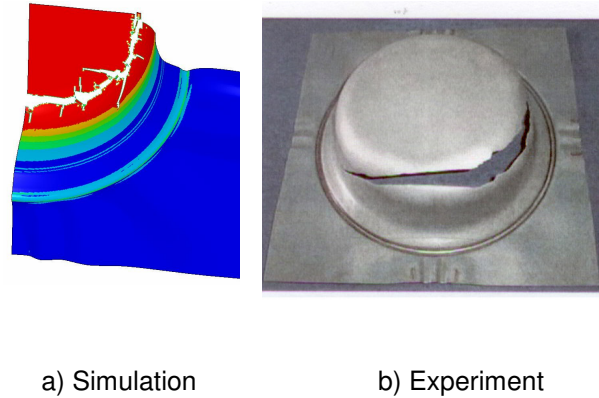


Figure 14: Damage pattern of Marciniak specimen in simulation (1/4 model) and experiment

### 4.3 Modelling of influences of pre-strain and pre-damage

To check the applicability of the damage model for loading cases with a pronounced change of triaxiality the tension and shear tests on specimens with pre-deformation under biaxial tension were simulated with the same damage parameters as applied in section 4.2. Figure 15 compares the nominal stress vs. strain curves of smooth and notched tension specimens cut from the original sheets and from Marciniak specimens which were loaded to 50% of the fracture strain. The numerical results in Figure 15 were obtained by using isotropic hardening. The influences of pre-deformation and change of triaxiality on deformation and fracture behaviour of smooth and notched tension specimens were well predicted.

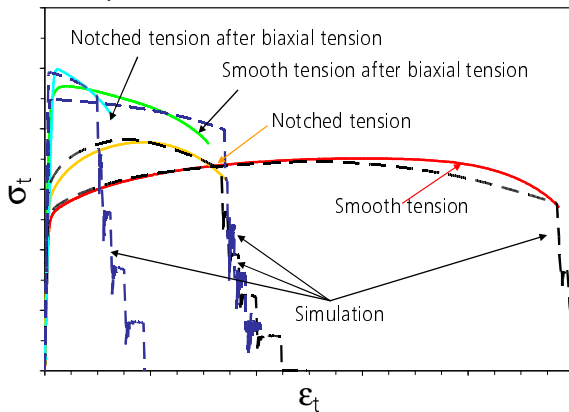


Figure 15: Influence of pre-deformation on nominal stress vs. strain curves of smooth and notched tension specimens

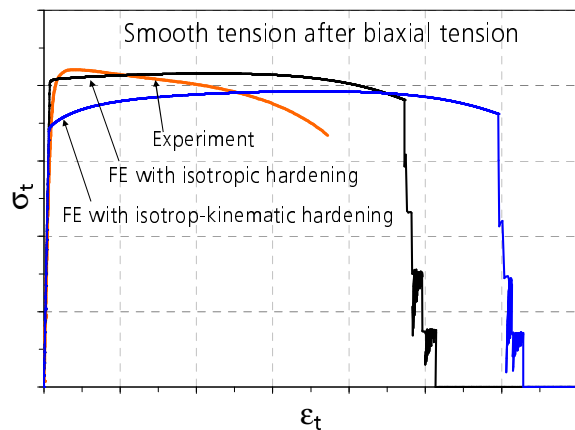


Figure 16: Measured and calculated nominal stress vs. strain curves of a smooth tension specimen with biaxial pre-deformation

Additionally, the material model for combined isotrop-kinematic hardening presented in section 3.2 was also applied to simulate the tests on specimens with pre-deformation. Figure 16 compares the results from both models for isotropic hardening and isotrop-kinematic hardening for the loading case with a smooth tension specimen which was cut from a Marciniak specimen loaded to 30% of fracture strain. It is interesting that the model for isotrop-kinematic hardening underestimates considerably the influence of pre-deformation under biaxial tension on the flow stress under uniaxial tension. The

different hardening behaviour of both material models results also in different localization behaviour (necking). Therefore, the model for isotrop-kinematic hardening predicts a much delayed rupture. According to the material model with isotrop-kinematic hardening specimens with biaxial pre-deformation should show a large difference in flow stress under tension and compression (see Figure 8). However, additional compression tests on specimens with pre-deformation performed in this work cannot confirm this effect. This means that it might be not necessary to use the material model for isotrop-kinematic hardening to make an integrated simulation from deep drawing to crash at least for this example. The main reason may be that stress signs for a material point during a Marciniak test are reversed maximum one time and the data of cyclic tests are not relevant for this case.

## 5 Validation tests on a component and crash simulation

### 5.1 Bending test with superposed tension

To validate the applied concept for damage modelling, component tests on a part of TRIP700 manufactured by deep drawing were performed. The component was loaded under bending with superimposed global tension to intensify the loading. Figure 17 and Figure 18 shows the damage pattern and the measured load vs. displacement curves of the components in comparison with numerical predictions. The first peak of the load vs. displacement curves is related to the beginning of folding of the component. Bending is the dominant load before reaching the minimum of the load and after that the superimposed tension is mainly responsible for further deformation.

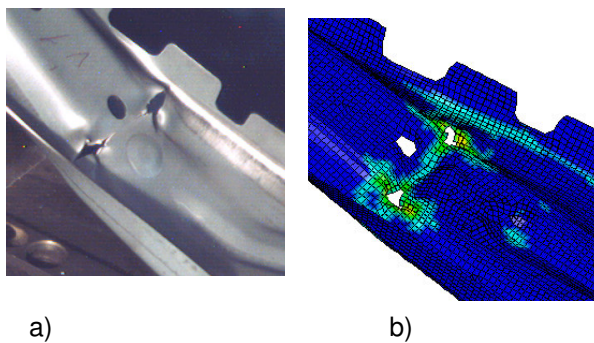


Figure 17: Damage pattern of a component  
a) experiment and b) simulation

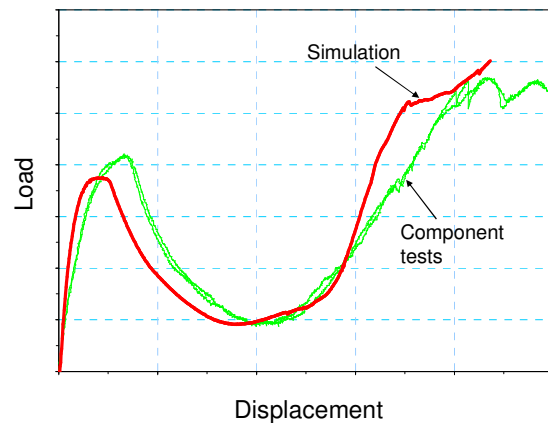


Figure 18: Measured and calculated load vs. displacement curves of component tests

### 5.2 Component simulation with mapped results from deep drawing to crash

The distributions of pre-strain, pre-damage and sheet thickness calculated from deep-drawing simulation were transferred to a crash model by using the mapping method available in LS-DYNA (DYNAIN-File). As element sizes for crash simulation are generally coarser than those for forming simulation and geometry deviations between two models exist due to cutting after deep drawing, the application of a mapping method is necessary. Figure 19 and Figure 20 compare the damage distributions before and after mapping.

The crash simulation of the components was performed on the basis of the damage parameters obtained from the original sheet and the mapped distributions of pre-strain, pre-damage and sheet thickness. The calculated damage pattern and load vs. displacement curve agree well with experimental results (Figure 17 and Figure 18). Additional simulations show that the first peak of load vs. displacement curve would be underestimated about 20% if the deformation history of deep drawing was not transferred to the crash model.

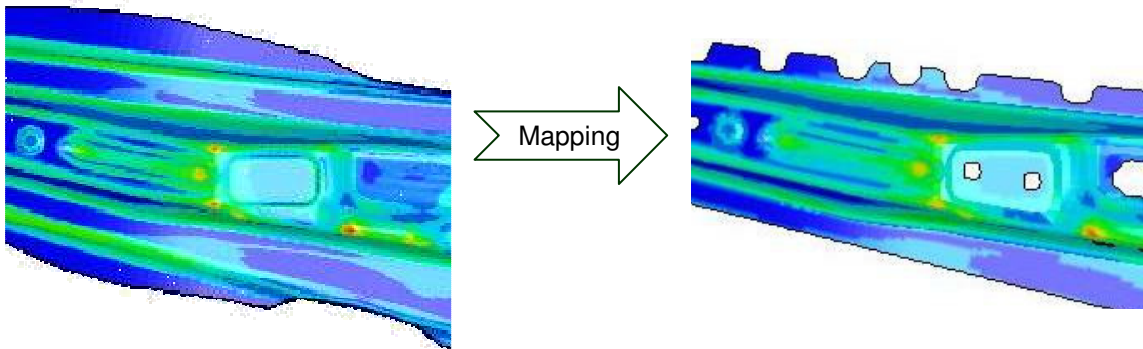


Figure 19: Distribution of damage in a component after deep drawing

Figure 20: Damage distribution in the crash model (after mapping)

## 6 Summary

The influence of pre-deformation and pre-damage caused by deep drawing on crash behaviour was characterized and simulated. An evaluation chain including relevant material characterization, numerical simulation with a suitable damage model and verification by component tests was conducted. The triaxiality was varied from shear to biaxial tension and loading path was changed from biaxial tension to uniaxial tension and shear. A specimen form enabling different shear-tension ratios was used to characterize damage behaviour between pure shear and tension. Cyclic tension-compression tests were conducted to determine material parameters for isotrop-kinematic hardening. A damage model describing both shear and dimple fracture was developed and applied for an integrated simulation from deep drawing to crash.

It was found that the material model with isotropic hardening is sufficient for coupling between deep drawing and crash simulations. The material model with isotrop-kinematic hardening is not relevant for this application. The influence of deformation history on damage was well predicted by the applied damage model. Component tests under bending with superimposed tension were used to validate the damage concept. The component simulation with the mapped distributions of pre-strain, pre-damage and sheet thickness shows a good agreement with the experimental results.

## 7 Literature

- [1] Werner, H., Dell, H., Metzmacher, G., Kessler, L., Heath, A., FLD-based failure model for coupled processes, EuroPAM, Mainz, 2003
- [2] Neukamm, F., Feucht, M., Haufe, A., Consistent damage modelling in the process chain of forming to crashworthiness simulations, 7. LS-DYNA Anwenderforum, 30. Sept.-1. Oct.2008 Bamberg
- [3] Zhu, H., Zhu, L., Chen, J.H., Lv, X.-F., Investigation of fracture mechanism of 6063 aluminum alloy under different stress states Int. J. Fract., 2007, 146, 159-172.
- [4] Barlat, F., Lian, J., Plastic behaviour and stretchability of sheet metals, Int. J. of Plasticity, Vol. 5, 1989, pp. 51-66
- [5] Lemaitre, J., Chaboche, J.L., Mechanics of Solid Materials, Cambridge University Press, 1990
- [6] Berstad, T., Langseth, M., Hoppenstad, O.S., Elasto-viscoplastic constitutive models in the explicit finite element code LS-DYNA3D, Second International LS-DYNA3D Conference, San Francisco, 1994
- [7] Bao, Y., Wierzbicki, T., On fracture locus in the equivalent strain and stress triaxiality space, Int. J. Mech. Sci., 2004, 46 (81), 81-98
- [8] Nahshon, K., Hutchinson, J.W., Modification of the Gurson Model for shear failure, Euro. J. Mech. A/Solids, 2008, 27, 1-17
- [9] Sun, D.-Z., Ockewitz, A., Klamsner, H., Malcher, D., Characterization and modeling of the deformation and damage behavior of aluminum materials for crash simulation, 11th International Conference on Aluminium Alloys Sept. 22-26, 2008 Aachen
- [10] Johnson, G.R., Cook, W.H., Fracture characteristics of three metals subjected to various strains, strain rates, temperatures and pressures, Engineering Fracture Mechanics, vol.21, No.1, 1985, pp.31-48